Tumor Growth Assessment by Computed Tomography Perfusion Imaging (CTPI), Perfusion-Weighted Imaging (PWI), and Diffusion-Weighted Imaging (DWI) in a Rabbit Pleural Squamous Cell Carcinoma VX2-Implanted Model

Authors' Contribution:
Study Design A
Data Collection B
Statistical Analysis C
Data Interpretation D
Manuscript Preparation E
Literature Search F
Funds Collection G

ABCDEF Qiang Zhang
ADE   Caixia Ba
BCE   Mingmin Zhang
BCD   Zhaoxin Liu
CD   Baoqi Shi
BF   Fuliang Qi
E   Haijiang Wang
D   Yuan Lv
D   Haijiao Jin
F   Xiaochuan Yang

Department of Radiology, Baotou Cancer Hospital, Baotou, Inner Mongolia, P.R. China

Corresponding Author: Caixia Ba, e-mail: caixiaba@tom.com
Source of support: Departmental sources

Background: Computed tomography perfusion imaging (CTPI) and perfusion-weighted imaging (PWI) are non-invasive technologies that can quantify tumor vascularity and blood flow. This study explored the blood flow information, tumor cell viability, and hydrothoraces in a rabbit pleural VX2-implanted model through use of CTPI, PWI, and DWI.

Material/Methods: A pleural VX2-implanted model was established in 58 New Zealand white rabbits. CTPI, PWI, and DWI were applied with a 16-slice spiral CT and an Archival 1.5 T dual-gradient MRI.

Results: Compared with muscle tissue, PV, PEI, and BV of parietal and visceral pleural tumor implantation rabbits showed significant differences. The t values of PV, PEI, and BV between parietal and visceral pleura were 2.08, 2.29, and 2.88, respectively. Compared with muscle tissue, WIR, WOR, and MAXR of parietal and visceral pleural tumor implantation rabbits showed significant differences. In parietal pleural tumor implantation rabbits, the section surface of lesion tissues was 5.2±2.7 cm². Hydrothorax appeared 6.0±2.0 days after tumor implantation. The mean value of ADC was 1.5±0.6. In visceral pleural tumor implantation rabbits, the section surface of lesion tissues was 1.6±0.8 cm². Hydrothorax appeared 7.0±3.0 days after tumor implantation. The mean value of ADC was 1.4±0.5. The t values of the above 3 indices for the parietal and visceral pleura were 1.85, 1.83, and 1.76, respectively ($P < 0.05$).

Conclusions: The combined application of CTPI, PWI, and DWI accurately and visually reflects the blood perfusion of tumor tissues and quantitatively analyzes blood flow information and the mechanism underlying hydrothorax generation in tumor tissues.

MeSH Keywords: Diffusion • Magnetic Resonance Imaging • Perfusion Imaging

Full-text PDF: https://www.medscimonit.com/abstract/index/idArt/909431

📄 3558   🖼 3   📊 4   📚 22

Background

Malignant tumors of the pleura are classified into primary tumors and metastatic tumors. The most common malignant pleural tumor is malignant pleural mesothelioma (MPM), which includes localized and diffused mesotheliomas. The localized MPM is well-differentiated and has low malignant potential. However, the diffused MPM is poorly-differentiated and has high malignant potential. Metastatic pleural tumors account for 95% of pleural tumors, and the majority are from lung and breast cancers, gastric cancer, pancreatic cancer, and primary uterine tumors. The least common primary focus of MPM is lymphoma. The incidence of MPM in the USA is 0.001% [1]. In China, the incidence is 0.0003–0.0005% [2]. The incidence of MPM has continued to rise across Europe [3]. The main components of multimodality treatment for MPM include surgery, chemotherapy, and radiation therapy. However, MPM is also associated with poor prognosis [4,5].

Computed tomography perfusion imaging (CTPI) and perfusion-weighted imaging (PWI) are non-invasive technologies that can quantify tumor vascularity and blood flow. CTPI and PWI can also quantitatively analyze the hemodynamic information in tumor tissues [6–8]. Angiogenesis is critical in tumorigenesis, development, infiltration, and metastasis of solid tumors. Angiogenesis significantly influences the biological behavior and prognosis of tumors [9–11]. The contrast medium of CTPI and PWI are mainly located inside and around vessels. Because the distribution of contrast medium determines the signal strength in normal and tumor tissues after enhancement, the distribution of contrast medium can directly indicate tissue perfusion and indirectly indicate microvascular distribution [12]. Diffusion-weighted imaging-MRI (DWI-MRI) is the only technique used to measure the motion of water molecules *in vivo*. The motion speed of water is expressed with an ADC value and quantified by DWI, which can indirectly indicate the status of cell proliferation [13]. CTPI, PWI, and DWI-MRI are widely used to monitor the different tumor progression stages.

In this study, we measured the perfusion parameters of CTPI and PWI and the ADC values of DWI to determine cell viability and hemodynamics of neovascularization in a rabbit pleural VX2-implanted model. Metastatic malignant tumors of the pleura always occur at TNM stage M1a and were accompanied by the generation of hydrothorax. We further explored the mechanism underlying hydrothorax formation.

Material and Methods

Animals and model establishment

Sixty-eight healthy New Zealand white rabbits of both sexes, weighing 2.5–3.0 kg, were purchased from the Experimental Animal Center of Beijing University (animal production permit number: S (Beijing) 2009-00140. Animals were fed under normal conditions.

The cell solution (0.3–0.5 ml at 2×10^7/ml) of VX2 (squamous cell carcinoma, provided by the Intervention Department of Peking University Cancer Hospital) was inoculated subcutaneously into 2 New Zealand white rabbits. Successful establishment of the tumor was determined by presence of palpable fixed subcutaneous soft tissue masses, which were further confirmed to be squamous cell carcinoma by pathology. Two weeks after inoculation, tumor cells were collected and suspended.

In 62 New Zealand white rabbits, artificial pneumothoraces were established at the right fourth and fifth intercostal spaces under CT guidance. Then, after a 0.5-ml suspension was injected into the pneumothorax, air was withdrawn. Then, 2 ml of gelatin was injected into the pleura. The rabbit pleural VX2-implanted model was successfully established in 58 rabbits and not established in 4 rabbits. Successful establishment of the model was determined by non-contrast CT scanning at the lung window, which showed local thickening of the pleura; DWI showed a local pleural high signal.

Fifty-eight rabbits were divided into the parietal group (n=12) and the visceral pleura groups (n=46). All rabbits were checked on the day of implantation, and once every other day until day 15 after implantation, with CTPI, DWI-MR, and PWI.

Scanning scheme and parameters

On the day of tumor cell implantation, experimental rabbits were fasted for 8 h. Before scanning, a venous indwelling needle was placed into the marginal ear vein. After being anesthetized with 0.1 mmol/l (1 ml/kg body weight) of pentobarbital sodium, rabbits were secured in the supine position. The static dynamic scan perfusion mode was applied in spiral CT. Lohexol contrast agent (3–4 ml of 350 mg/ml) was injected intravenously through a double-syringe power injector at 0.4 ml/s. CT scanning in the continuous volume scan mode was started 1 s after injection. The static dynamic scan perfusion mode was applied in MRI. The contrast agent, Gd-DPTA (2–3 ml), was injected intravenously through a high-pressure injector at 0.3 ml/s. MRI scanning with the continuous volume scan mode was started 1 s after injection. The scanning parameters were as follows: MRI coil, Sense-Body; DWI/ADC parameters, FOV 120 mm, TR2529, TED55, TI180, NSA16, and thickness 1.5 mm; and PWI parameters, FOV 120 mm, TR4.4, TE2.2, Flip10, NSA1, and thickness 1 mm.

CTPI and PWI methods

The following were regions of interest (ROI): aorta; tumor tissue; and ipsilateral muscle tissue.

The ROI selection method was as follows: select the aorta, tumor tissue, and ipsilateral muscle tissue from the same patient; and measure the perfusion value (PV), peak enhanced increment (PEI), transit time peak (TTP), blood volume (BV), wash-in rate (WIR), wash-out rate (WOR), maximum enhancement rate (MAXR), transit time peak (TTP), and apparent diffusion coefficient (ADC). Specific perfusion software and the EBW 4.0 workstation were used as CT image post-processing. Specific perfusion software and Workspace workstation were used as MRI post-processing. The CTPI and PWI pictures obtained from the above software were used to analyze the viability of tumor cells and blood perfusion of tumor tissues.

DWI measurement, MRI coil, and Sense-Body

The ADC value was measured at the high DWI signal area. The ADC-duration and ADC-maximum section surface curves of lesion tissues were created. Cell viability was assessed during tumor progression.

Detection of hydrothoraces

From the time that a hydrothorax was detectable, the largest depth of the pleural effusion was semi-quantified by the distance between layers of the parietal and visceral pleura on the CT or MRI axial image. Tumor growth speed and site were determined by a hydrothorax generation curve.

Immunohistochemistry

Using the streptavidin peroxidase method, brown staining of endothelial cells indicated CD34-positive cells. Five independent areas were selected under a 200×field and CD34-positive vessels were counted in each of these areas. The intensity of expression was evaluated as follows: 5% positive cells was considered (–); 5–25% positive cells was (+); 26–50% positive cells was (++); and 51–100% positive cells was (+++). Microvessel density was measured by anti-CD34 staining.

Statistical methods

All data were analyzed using SPSS13.0 software. The independent-samples t test was used to analyze the perfusion parameters of CTPI and PWI, ADC values, section surfaces of lesion tissues, and time period of hydrothorax appearing after tumor inoculation. $P < 0.05$ and $P < 0.01$ were considered statistically significant differences.

Results

The establishment of a rabbit pleural VX2-implanted model

In the early stage of tumorigenesis, local thickening of the pleura was observed with CT. Then, nodules were found in visceral pleura (single or multiple and circular or quasi-circular, with a complete capsule). The nodules were also found in the parietal pleura, which had an irregular shape and an incomplete capsule or no capsule. Within the parietal pleura, nodule fusion in chains occurred with widespread irregular pleural thickening or generation of an irregular soft-tissue mass. The relative place of the tumor and visceral or parietal pleura could be determined clearly in T2 lipid suppression images. Hydrothoraces showed uneven high signals (Figure 1A1, 1B1).

CTPI parameters of ROIs in the rabbit pleural VX2-implanted model

As shown in Table 1, based on an analysis with paired t tests and compared with muscle tissue, the t values of PV, PEI, and BV of parietal pleural tumor implantation rabbits were 6.28, 5.79, and 6.88, respectively ($P<0.01$). Based on an analysis with independent-samples t tests and compared with muscle tissue, the t values of PV, PEI, and BV of visceral pleural tumor implantation rabbits were 3.67, 2.94, and 3.55, respectively ($P<0.01$). The t value of TTP for the parietal and visceral pleura compared with muscle were 2.21 and 1.65, respectively ($P>0.05$). Based on an analysis with the t test for 2 samples, the t values of PV, PEI, and BV between parietal and visceral pleura were 2.08, 2.29, and 2.88, respectively ($P<0.05$), and the t value of TTP was 1.57 ($P>0.05$). CTPI in the rabbit pleura VX2 tumor implantation model showed that in the early stage of tumorigenesis, local thickening of the pleura was observed. CT perfusion showed a very low perfusion volume. All of the values for PV, PEI, TTP, and BV were very low. The shape of the curve was straight. When the tumor diameter was >0.35 cm, nodules were noted in the pleura on CT images with medium-low perfusion volumes. All of the values for PV, PEI, TTP, and BV were medium-low. There were progressive fluctuations in the curve. When the tumor diameter was >0.85 cm, CT perfusion showed a high perfusion volume. All of the values of PV, PEI, TTP, and BV reached peak values. The curve became sharp and steep. When the tumor diameter was >1.45 cm, there were liquefactive necrosis areas in the central tumor with low or very low perfusion volumes. At the rim of the tumor all of the values rose slowly (Figure 1A2–1A5).

PWI parameters of ROI in rabbit pleural VX2 implanted model

As shown in Table 2, based on an analysis with an independent-samples t test and compared with muscle tissue, the t values
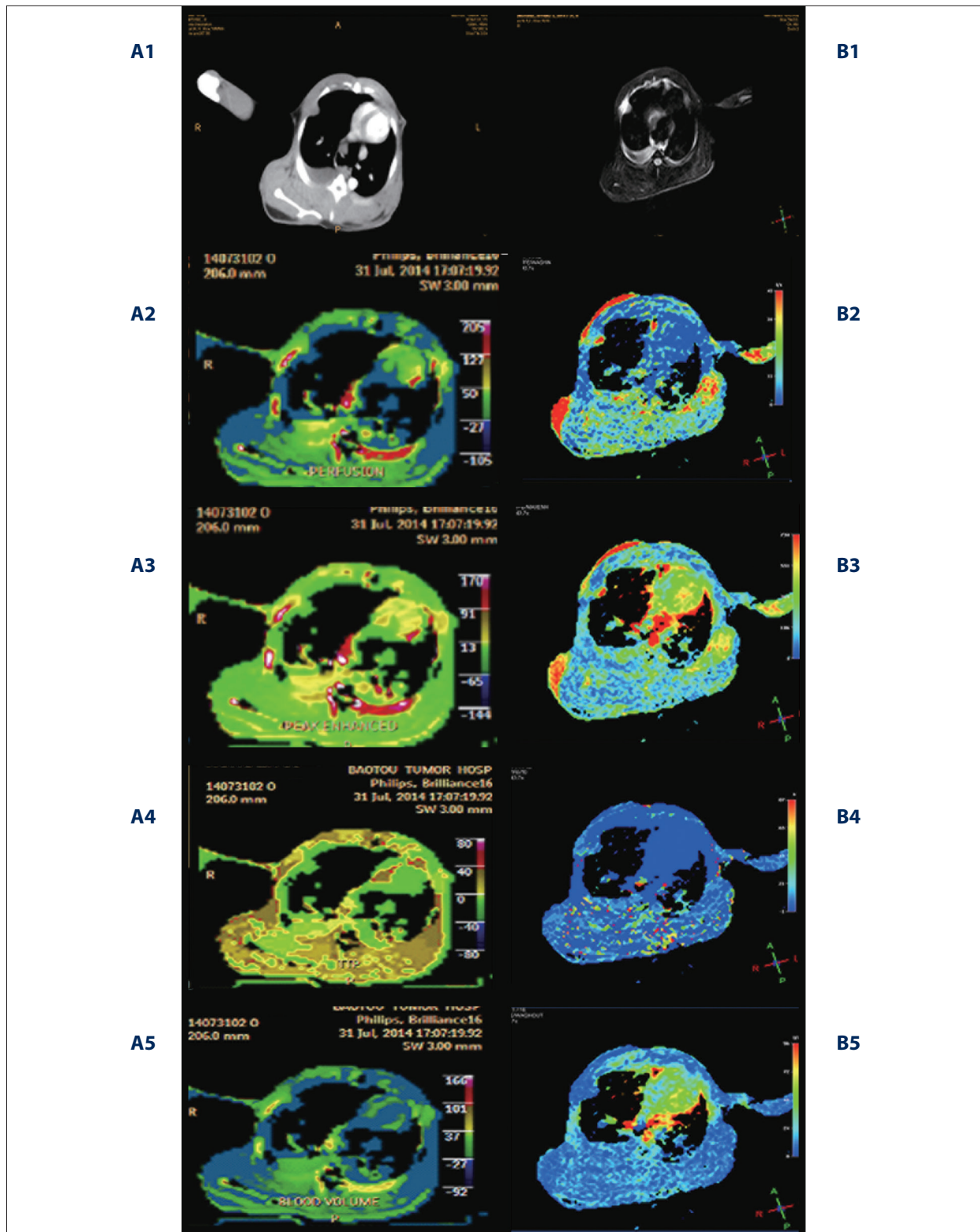
Figure 1. CT-enhanced scanning showed nodular shadow (**A1**). In T2 lipid suppression image, nodules infiltrated in surrounding pleura with uneven hydrothorax signal presented in **A2–A5** CTPI parameter image: PV (**A2**), PEI (**A3**), TTP (**A4**), BV (**A5**). (**B2–B5**) PWI parameter image, WIR (**B2**), WOR (**B3**), TTP (**B4**), MER (**B5**). All parameters in tumor tissues were higher than in normal muscle tissues.

Table 1. Parameters of CT perfusion image in VX2 pleura implantation rabbit model.

Group	PV	PEI	TTP	BV
Tumor in parietal pleura	34.35±5.46	38.60±4.05	45.33±8.50	31.86±6.82
Tumor in visceral pleura	29.04±2.19	32.29±6.31	45.36±7.85	18.21±3.75
Muscle	16.94±5.39	21.89±7.29	45.48±9.65	7.14±4.45

Perfusion volume (PV), peak enhanced increment (PEI), transit time peak (TTP), and blood volume (BV).

Table 2. Parameters of MRI perfusion image in VX2 pleura implantation rabbit model.

Group	WIR	WOR	TTP	MER
Tumor in parietal pleura	49.41±14.19	30.42±9.76	66.39±18.54	980.34±60.89
Tumor in visceral pleura	41.09±12.28	23.47±5.10	66.48±2.20	921.76±58.72
Muscle	24.09±5.29	7.47±5.11	65.48±12.21	504.76±53.73

Wash in rate (WIR), wash out rate (WOR), maximum enhancement rate (MAXR), and transit time peak (TTP).

of WIR, WOR, and MAXR for parietal pleural tumor implantation rabbits were 7.42, 6.27, and 7.95, respectively ($P<0.01$). Based on an analysis with an independent-samples t test and compared with muscle tissue, the t values of WIR, WOR, and MAXR for visceral pleural tumor implantation rabbits were 3.04, 3.94, and 2.95, respectively ($P<0.01$). The t value for TTP of the parietal and visceral pleura compared with muscle were 2.11 and 1.59, respectively ($P>0.05$). Based on an analysis with the t test for 2 samples, the t values of WIR, WOR, and MAXR between parietal and visceral pleura were 2.13, 2.34, and 2.21, respectively ($P<0.05$), and the t value for TTP was 1.70 ($P>0.05$). The PWI results in the rabbit pleura VX2 tumor implantation model showed that in the early stage of tumorigenesis, MR perfusion was not clear. When the tumor diameter was >0.35 cm, the MR perfusion volume increased gradually from a medium-low level. All of the values of WIR, WOR, MER, and TTP were low. There were progressive fluctuations and slow up-lifting in the curve. When the tumor diameter was >0.85 cm, the MR perfusion volume was high. All of the values of WIR, WOR, MER, and TTP were high, but with a gradual up-lifting trend and fluctuation. The curve reached the peak platform with a wavy up-lifting shape. When the tumor diameter was >1.45 cm, the tumor center had no or a very low perfusion volume, but at the rim of the tumor all of the values rose slowly (Figure 1B2–2B5).

DWI representation in rabbit pleural VX2 implanted model

At the early stage of tumorigenesis, DWI showed linear high-intensity signals. When nodules were generated in the tumor tissues, the DWI signals gradually increased. The ADC signals were very low in the center of the tumor tissues, but high at the rim of the tumor tissues. Most of the lesions in visceral

pleura were localized, while the lesions in parietal pleura were irregularly diffuse. When the tumor diameter were >0.85 cm, the DWI signals gradually increased to a maximum value and clearly showed a broader tumor. The ADC signals were low at the center of the lesion tissues and high at the rim of the tumor and surrounding tissues. When a hydrothorax was generated, the hydrothorax had no DWI signal, but had an uneven high signal in the ADC image. When the tumor diameter was >1.45 cm, there were areas of liquefactive necrosis in the tumor center with low DWI and ADC signals. With respect to the rim of the lesions, DWI signals were very high, but increased slowly, while the ADC signals were very low (Figure 2A, 2B).

The relationship between the size of the pleura implantation tumor, ADC value, and time of hydrothorax appearance

The relationship between the size of the pleura implantation tumor, ADC value, and time of hydrothorax appearance are shown in Table 3. The maximum cross-section area, time of hydrothorax appearance, and ADC mean value were analyzed with the t test for 2 samples. Seventy-two tumors were implanted in the parietal pleura and 276 were in the visceral pleura. Based on the independent-samples t test, the t value for the maximum cross-section area, time of hydrothorax appearance, and ADC mean value were 1.85, 1.83, and 1.76, respectively ($P<0.05$). At the early stage of tumorigenesis, the maximum cross-section area in the parietal and visceral pleura was 0.12–2 cm². The ADC decreased rapidly from 2.6×10^{-3} mm²/s to 1.2×10^{-3} mm²/s (visceral pleura) and from 2.4×10^{-3} mm²/s to 1.5×10^{-3} mm²/s (parietal pleura). When the tumor grew gradually, the ADC value varied from 1.2×10^{-3} to 1.5×10^{-3} mm²/s (Figure 3A).
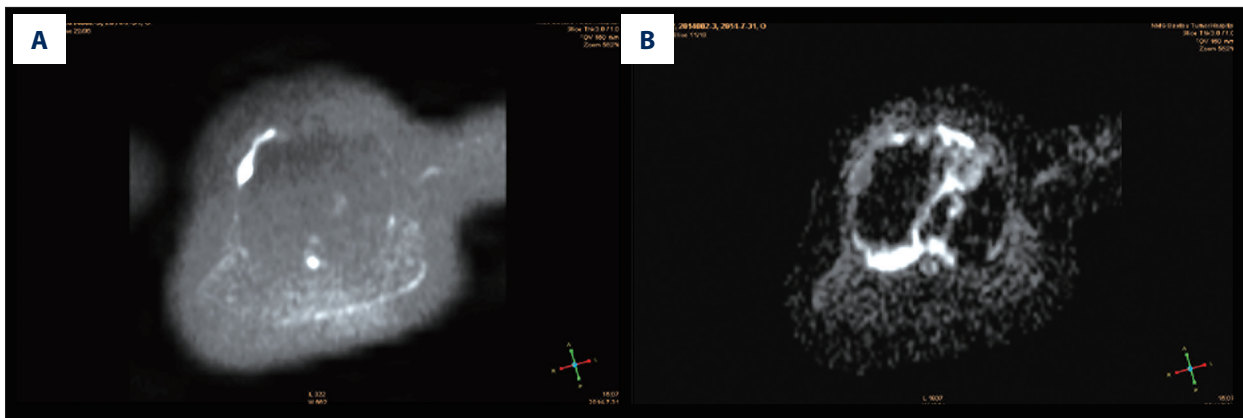
Figure 2. (**A**) DWI picture. The signal was high and the surrounding pleura was infiltrated. (**B**) ADC picture, the signal was very low at the center of the nodule in the pleural cavity. The signal was relatively higher at the rim of the nodule.

Table 3. The size of the pleura implantation tumor, ADC value, and time of hydrothorax appearance.

	Case number	Maximum cross-section area (cm²)	Time of hydrothorax appearance (day)	ADC mean value
Tumor implanted in parietal pleura	12	5.2±2.7	6.0±2.0	1.5±0.6
Tumor implanted in visceral pleura	46	1.6±0.8	7.0±3.0	1.4±0.5

Within 7 days from the time at which the implanted tumor was detectable, the ADC decreased rapidly from 2.6×10^{-3} to 1.2×10^{-3} mm²/s (visceral pleura) and from 2.4×10^{-3} to 1.5×10^{-3} mm²/s (parietal pleura). With time, the ADC value tended to be stable, varying from 1.2×10^{-3} to 1.5×10^{-3} mm²/s (Figure 3B). Hydrothoraces appearing 5 days after the implanted tumor were detected. The volume of the hydrothorax in rabbits implanted with tumor in the parietal pleura was higher than in rabbits implanted with tumor in the visceral pleura. On day 9, the hydrothorax in the parietal pleura was 2.7 cm and 1.6 cm in the visceral pleura (Figure 3C).

The expression change of VEGF in the rabbit pleural VX2 implanted model

Immunohistochemistry was used to detect the expression of VEGF. When the tumor diameter reached 0.35 cm (0.10 cm²), tumor tissues in the parietal and visceral pleural were VEFG (+). When the tumor diameter reached 0.85 cm (0.74 cm²), tumor tissues in the parietal pleura were VEFG (++), while tumor tissues in the visceral pleura were VEFG (+). When the tumor diameter reached 1.45 cm (2.10 cm²), tumor tissues in the parietal pleura were VEFG (+++), tumor tissues in the visceral pleura were VEFG (++), and the center of the tumor tissues in the parietal pleura were VEFG (–). Along with the increase in tumor size, the ADV value decreased, but VEGF expression and MVD increased (Figure 4).

Discussion

In the present study, the rabbit VX2 pleura implantation model was successfully established in 90.63% of the cases (20.69% in the parietal pleura and 79.31% in the visceral pleura). A high proportion of implanted tumors were in the parietal pleura, which might be related to the difference in osmotic pressure among the capillaries in the parietal and visceral pleura, because the former had a higher pressure. The visceral pleura receives blood supply from the bronchial circulation. The parietal pleura receives blood supply from the posterior intercostal arteries. Between 3 and 11 posterior intercostal arteries connect the internal thoracic artery and musculophrenic artery at the costophrenic angle. A gradient for fluid formation is normally present in the parietal pleura.

We also found that there was no neovascularization at the early stage with less tissue expression of VEGF (+). The growth of implanted tumor tissue in the visceral pleura was mainly dependent on the fluid in the pleural cavity, but not a direct blood supply. The number of microvessels or MVD in the parietal pleura tumors was higher than in the visceral pleura. The microvessels absorb nutrients from the branch of the intercostal artery and fluid in the pleural cavity. The viability of tumor cells was very low, with an ADC value of 2.4 to 2.6×10^{-3} mm²/s. Kinoshita et al. reported a significant correlation between the ADC of the tumor tissue and cell density [14].
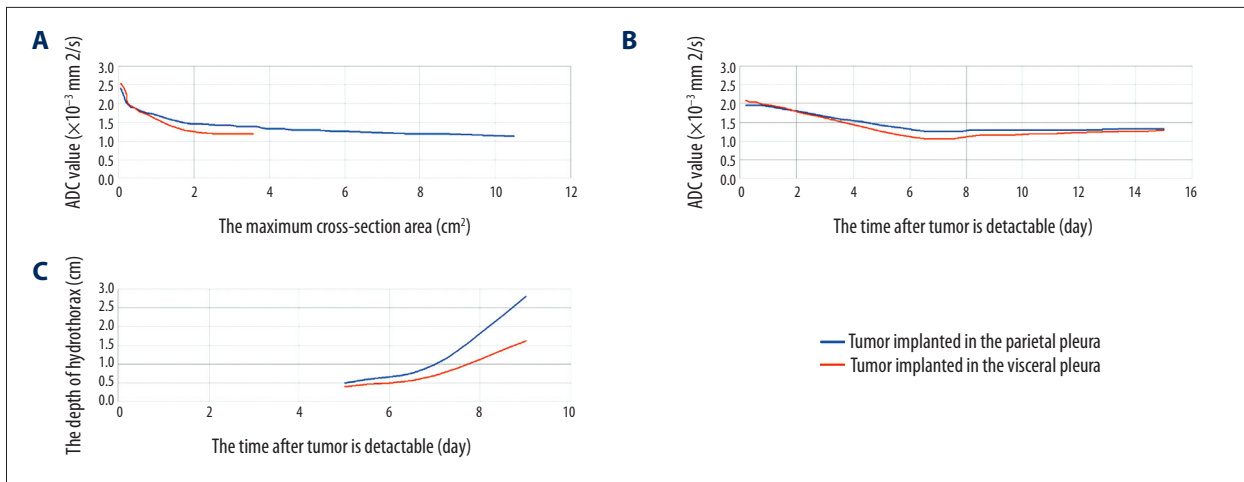
Figure 3. (**A**) Shows the relationship between the ADC value and maximum cross-section area; (**B**) Shows the relationship between the ADC value and time; (**C**) Shows the depth of hydrothorax after the tumor is detectable.
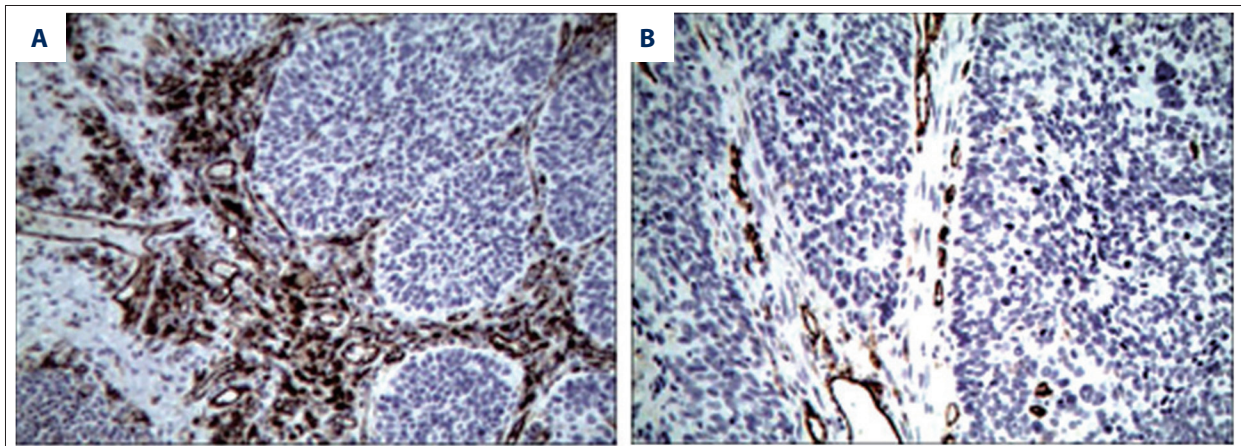

Figure 4. The immunoreactivity of VEGF in tumor tissues of the parietal and visceral pleura.

In the early stage of malignant pleura tumor progression, local thickening of the pleura occurred. As the tumor cells grow, nodules or tissue masses are generated [15]. Metastatic nodules in visceral pleura can be clearly observed by CT. In the lung window, nodules 2–3 mm in size can be identified by small nodular shadows or a rough surface on the lung. The sensitivity can be 75–100% [16,17]. In the present study, the tumor implanted in the visceral pleura grew more slowly than the tumor implanted in the parietal pleura, with a less than maximum cross-section area.

MRI can be used to accurately assess tumor infiltration in the pleura and chest [18]. In the present study, DWI showed a high linear signal in the early stage of tumor progression. The DWI signal of the nodule gradually increased to the peak value. Compared with CTPI or PWI, DWI can more easily show the change in the lesion area and surrounding tissues. The area of the lesion was larger than the area in the perfusion image, which reflected infiltration of the tumor in the surrounding

tissues and the change in the tumor microenvironment, even in the early stage of tumor progression.

With growth of the tumor, neovascularization becomes apparent and cells showed higher VEGF (++) expression. Cells become more aggressive. The tumor showed infiltrative growth with an incomplete capsule, a larger gap between vascular endothelial cells, higher osmotic pressure, malignant tumor cells, and increased blood perfusion [19]. Lesions in the visceral pleura were single or multiple, and circular or quasi-circular with incomplete capsule. Lesions in the parietal pleura were often multiple, irregular in shape, with an incomplete capsule or no capsule, and sometimes fused in a chain. Because there were a sufficient number of vessels in the parietal pleura, tumors in the parietal pleura grew quickly along the chest muscles, with an irregular shape, sometimes in chains with widespread irregular pleural thickening or generation of irregular soft-tissue masses.

At different stages of tumor progression, CTPI and PWI had different parameters [20]. In the present study, 7 days from the time at which the implanted tumor was detectable, the ADC value decreased quickly and the number of new vessels increased. All values of PV, PEI, BV, WIR, WOR, and MER were elevated (P<0.01). On day 7, all the values changed. The highest percentage of cell viability and the lowest ADC and VEGF (+++) were detected. At the early stage of tumor progression, PWI was not clear, while CTPI had very low perfusion. When the tumor diameter was >0.5 cm, PWI perfusion increased gradually from medium to low. When the tumor diameter was >1 cm, CTPI and PWI had high perfusion and sufficient information about the lesion. When the tumor diameter was >1.5 cm, there was no or very low perfusion in the center of the tumor tissue. The parameter at the rim of the tumor tissue increased slowly.

In the normal parietal pleura, there are 100 lymphatic stomata per cm^2. In the normal visceral pleura, there are 8000 lymphatic stomata per cm^2. The aperture of lymphatic ducts was 2–12 μm. Hydrothoraces could be reabsorbed by lymphatic vessels through lymphatic stomata. When the tumor infiltrates or transfers to the pleural cavity, inflammation occurs. This is always accompanied with pleuritis, angiogenesis, high vascular permeability, and generation of a pleural effusion [21,22]. This is the most common reason why a malignant tumor is accompanied by hydrothorax. Zhang et al. reported that metastasis to the lymph nodes and vessels occurred with tumor growth, which was accompanied by increasing WIR, increasing intra-tumoral interstitial pressure, increasing WOR, and the generation of hydrothorax caused by tumor cell infiltration to adjacent vessels or lymph nodes [20]. In the present study, the generation of a hydrothorax in the pleural tumor-implanted rabbits was directly related with tumor size, infiltration of lymph-vessels, and the place and range of infiltration.

Generally, a hydrothorax appeared 5 days after the tumor mass was detectable, and gradually increased. The animals with tumor implanted in the parietal pleura had higher cell viability, larger size, and a hydrothorax that increased from day 7. This is related to the obstruction or compression of lymph-vessels which blocked lymphatic drainage. The tumors implanted in the visceral pleura grew slowly because the pleura is closed to lung tissue with fewer vessels. As a result, less hydrothorax volume was generated. The generation of a hydrothorax was increased only when the tumor mass was developed to compress the lymph-vessels. On day 9, the hydrothorax was 2.7 cm in the rabbits with tumors implanted in the parietal pleura, which is much larger than in rabbits with tumors implanted into the visceral pleura (1.6 cm).

Diffuse malignant pleura tumor had a very bad prognosis with a very high mortality. Most patients die several months after clinical symptoms appear. Currently, there is no effect of chemotherapy or radiotherapy. Patients with diffuse tumor are not candidates for surgery. The biological features of the tumor are crucial for the treatment effect. Precise measurement of tumor cell viability, hemodynamic parameters, growth rate, and the basis for hydrothorax generation are key factors. The combined application of CTPI, PWI, and DWI can non-invasively reflect the real biological features of tumor tissues. This application will provide information for clinical treatment of malignant tumors in the pleura.

Conclusions

The combined application of CTPI, PWI, and DWI accurately and visually reflects the blood perfusion of tumor tissues and quantitatively analyzes blood flow information, which will be valuable to monitor the different tumor progressive stages.

References:

1. Chen SE, Pace MB: Malignant pleural mesothelioma. Am J Health Syst Pharm, 2012; 69: 377–85
2. Helland A, Solberg S, Brustugun OT: Incidence and survival of malignant pleural mesothelioma in norway: A population-based study of 1686 cases. J Thorac Oncol, 2012; 7: 1858–61
3. Jennings CJ, Walsh PM, Deady S et al: Malignant pleural mesothelioma incidence and survival in the Republic of Ireland 1994–2009. Cancer Epidemiol, 2014; 38: 35–41
4. Takuwa T, Hasegawa S: Current surgical strategies for malignant pleural mesothelioma. Surg Today, 2016; 46: 887–94
5. Schirren M, Sponholz S, Oguzhan S et al: [Surgical therapy of malignant pleural mesothelioma]. Chirurg, 2016; 87: 455–66 [in German]
6. Chen YW, Pan HB, Tseng HH et al: Assessment of blood flow in hepatocellular carcinoma: Correlations of computed tomography perfusion imaging and circulating angiogenic factors. Int J Mol Sci, 2013; 14: 17536–52
7. Malavasi S, Barone D, Gavelli G, Bevilacqua A: Multislice analysis of blood flow values in CT perfusion studies of lung cancer. Biomed Res Int, 2017; 2017: 3236893
8. Lv Y, Jin Y, Xu D et al: Assessment of 64-slice spiral computed tomography with perfusion weighted imaging in the early diagnosis of ground-glass opacity lung cancer. J BUON, 2016; 21: 954–57
9. Li Q, Wu T, Jing L et al: Angiogenesis inhibitors for the treatment of small cell lung cancer (SCLC): A meta-analysis of 7 randomized controlled trials. Medicine (Baltimore), 2017; 96: e6412
10. Nefedova NA, Kharlova OA, Danilova NV et al: [Markers of angiogenesis in tumor growth]. Arkh Patol, 2016; 78: 55–63 [in Russian]
11. Villaruz LC, Socinski MA: The role of anti-angiogenesis in non-small-cell lung cancer: An update. Curr Oncol Rep, 2015; 17: 26
12. Li JL, Ye WT, Liu ZY et al: Comparison of microvascular perfusion evaluation among IVIM-DWI, CT perfusion imaging and histological microvessel density in rabbit liver VX2 tumors. Magn Reson Imaging, 2018; 46: 64–69
13. Yuan YH, Xiao EH, Liu JB et al: Gene expression and MR diffusion-weighted imaging after chemoembolization in rabbit liver VX-2 tumor model. World J Gastroenterol, 2008; 14: 5557–63; discussion 5562
14. Kinoshita M, Arita H, Okita Y et al: Comparison of diffusion tensor imaging and (11)C-methionine positron emission tomography for reliable prediction of tumor cell density in gliomas. J Neurosurg, 2016; 125: 1136–42

15. Yang ZG, Sone S, Takashima S et al: High-resolution CT analysis of small peripheral lung adenocarcinomas revealed on screening helical CT. Am J Roentgenol, 2001; 176: 1399–407

16. Bakhshayesh Karam M, Karimi S, Mosadegh L, Chaibakhsh S: Malignant mesothelioma versus metastatic carcinoma of the pleura: A CT challenge. Iran J Radiol, 2016; 13: e10949

17. Reetz JA, Buza EL, Krick EL: CT features of pleural masses and nodules. Vet Radiol Ultrasound, 2012; 53: 121–27

18. Koegelenberg CF, Diacon AH: Image-guided pleural biopsy. Curr Opin Pulm Med, 2013; 19: 368–73

19. Zhang Q, Qian H: [Studies on lung cancer angiogenesis – application of interventional therapy (a report of 56 cases).] Chinese Journal of Clinical Oncology, 2007; 4: 61–64 [in Chinese]

20. Zhang Q, Shi B, Liu Z et al: Preliminary study of CT in combination with MRI perfusion imaging to assess hemodynamic changes during angiogenesis in a rabbit model of lung cancer. Onco Targets Ther, 2013; 6: 685–92

21. Neragi-Miandoab S: Malignant pleural effusion, current and evolving approaches for its diagnosis and management. Lung Cancer, 2006; 54: 1–9

22. Stathopoulos GT, Sherrill TP, Karabela SP et al: Host-derived interleukin-5 promotes adenocarcinoma-induced malignant pleural effusion. Am J Respir Crit Care Med, 2010; 182: 1273–81